Article

An Ediacaran orogeny in subglacial East Antarctica is uncovered by detrital garnet geochronology

Check for updates

Sharmaine Verhaert [1] ✉, Stijn Glorie [1], Martin Hand[1], Jacob A. Mulder[1], Anthony R. Milnes [1] & Jacqueline A. Halpin[2,3]

Detrital minerals provide valuable insights into the tectonic history of continents. Uranium-lead dating of detrital zircon is widely used to characterize the magmatic history of continents but is generally insensitive to metamorphism accompanying the production and reworking of crust during orogenesis. Garnet is the most important mineral for recording prograde and peak orogenic metamorphism and can occur as a common detrital phase. Here, we demonstrate laser-ablation lutetium-hafnium (Lu–Hf) geochronology of detrital garnet as a provenance tool for reconstructing orogenic histories at (super) continental scales. Detrital garnet (n = 557) from modern sands and Permo-Carboniferous glacial strata in South Australia faithfully record local garnet-grade metamorphic events but also include a major population at ca. 590 million-years with no known source in South Australia. We trace the ca. 590 million-year-old detrital garnets to a largely ice-covered orogenic province in East Antarctica, uncovering the inception of convergent margin tectonism along the palaeo-Pacific margin of Gondwana.

Clastic sediments preserve important records of the tectonic history of continents because they sample large crustal domains, including areas that are poorly exposed or difficult to access. Although detrital zircon uranium–lead (U–Pb) dating has emerged as a cornerstone of contemporary tectonic analysis[1], some fundamental tectonic processes are poorly captured by the detrital zircon archive. Specifically, regional metamorphism accompanying orogenesis contributes little detrital zircon to surrounding sedimentary basins due to the low fertility of zircon in most sub-solidus metamorphic rocks[2,3]. The insensitivity of detrital zircon to metamorphic events is a particularly important shortcoming for studying the tectonic history of continents because orogenesis is fundamental to creating, stabilising, and modifying continental crust[4]. Harnessing detrital mineral proxies that are sensitive to the metamorphic history of orogenic events, therefore, remains an outstanding challenge for unravelling the tectonic history of continents from the clastic sedimentary record[3,5,6].

Garnet is arguably the most important mineral for reconstructing orogenic histories[7,8]. Garnet crystallises in a wide range of metamorphic systems and uniquely provides a direct time-integrated record of the (prograde) pressure and temperature history of metamorphic rocks, which in turn reflect the first-order orogenic processes governing the thickness and thermal state of the lithosphere[7,9,10]. The ability of garnet to record prograde

metamorphic conditions offers an advantage over other routinely dated metamorphic minerals such as mica (argon–argon; Ar–Ar) or apatite (U–Pb, fission track), which generally record post-peak metamorphic cooling events due to the lower isotopic closure temperatures of these mineral chronometers[11].

Garnet can occur as a common accessory detrital mineral in continentally derived clastic sediment and is best preserved in settings that have experienced minimal chemical weathering[12,13]. Garnet is also enriched in rare earth elements, making it highly amenable to dating via the samarium–neodymium (Sm–Nd) and lutetium–hafnium (Lu–Hf) isotopic systems[9]. The Lu–Hf system in garnet is highly robust against thermal disturbances and REE loss, establishing garnet Lu–Hf geochronology as a reliable method to date garnet growth and recrystallisation in metamorphic rocks, even when (ultra)high-temperature overprinting has occurred[14,15]. This makes garnet Lu–Hf geochronology a crucial dating method for studying the tectono-metamorphic history of orogenic systems[15]. However, detrital garnet geochronology via traditional solution-based techniques (e.g., Sm–Nd and Lu–Hf) is unrealistic, given the labour-intensive nature of these methods. For example, a previous solution-based detrital garnet study[16] generated 19 single-grain Sm–Nd ages, which falls well below the >100 ages per sample benchmark considered in most provenance studies as sufficient

[1]Department of Earth Sciences, School of Physical Sciences, The University of Adelaide, Adelaide, SA 5005, Australia. [2]Institute for Marine and Antarctic Studies, University of Tasmania, Hobart, TAS 7001, Australia. [3]The Australian Centre for Excellence in Antarctic Science, University of Tasmania, Hobart, TAS 7001, Australia. ✉e-mail: sharmaine.verhaert@adelaide.edu.au
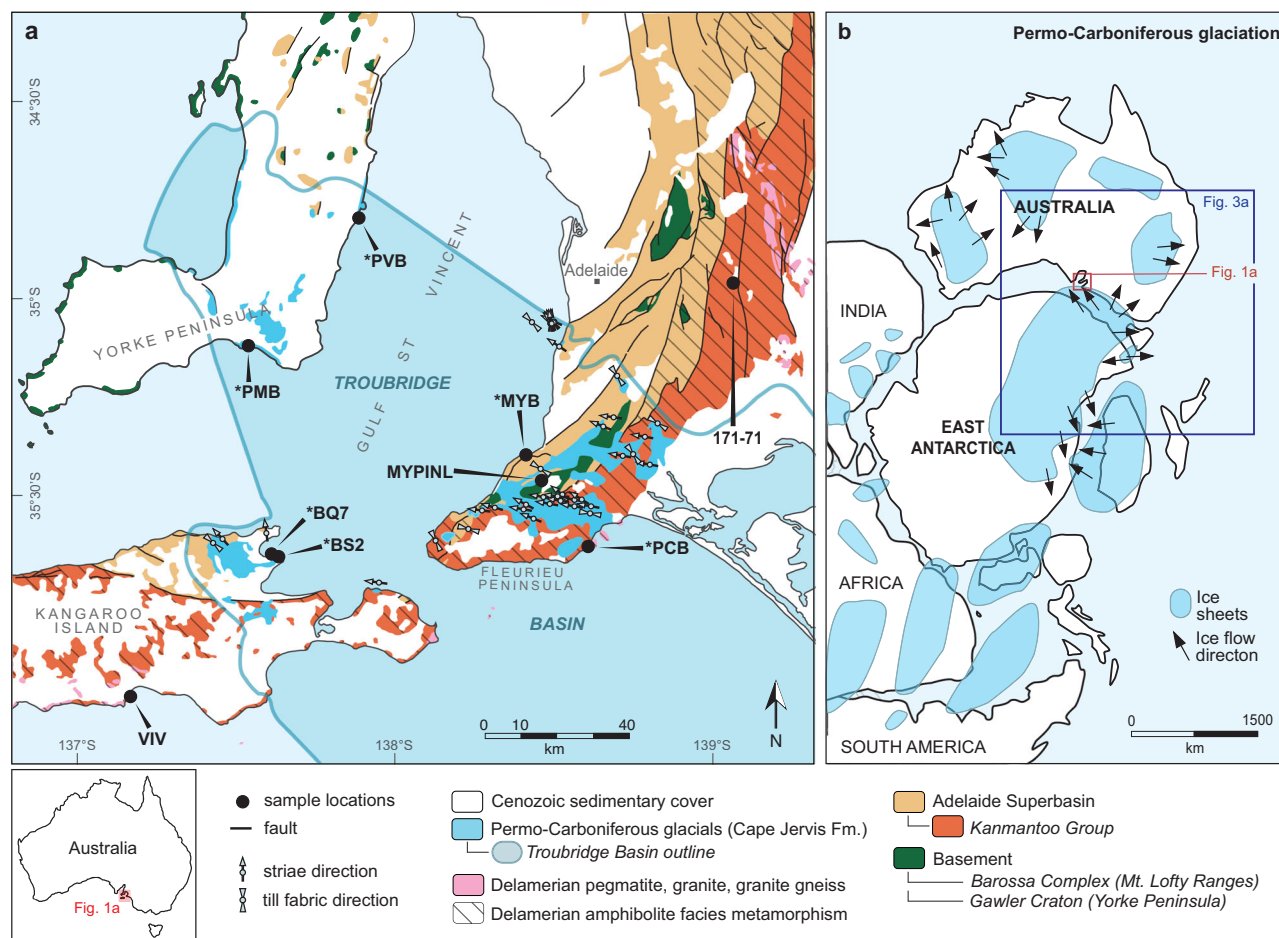
Fig. 1 | Regional geological map with sample locations and configuration of Gondwana during the Late Palaeozoic Ice Age. a Simplified geological map of Fleurieu Peninsula, Yorke Peninsula and Kangaroo Island in South Australia[24,79,80]. The geological map illustrates the extent of the Permo-Carboniferous Troubridge Basin (outlined in blue) and known paleo ice-flow indicators[29]. The asterisk (*) indicates the detrital garnet-rich placer sand and glacial strata samples, and samples without an asterisk are local basement rocks. The garnet-rich placer deposit samples come from four beaches in South Australia: Myponga Beach (sample MYB), Petrel Cove Beach (PCB), Port Moorowie Beach (PMB) and Port Vincent Beach (PVB). The two Permo-Carboniferous glacial strata (samples BS2 and BQ7) are from the

Cape Jervis Formation on Kangaroo Island, which locally also contains detrital garnet[41]. Additionally, three basement samples were analysed to define regional garnet populations: a Barossa Complex granulite from the Myponga Inlier in the Adelaide Hills (MYPINL), a Delamerian metapelite from Harrogate (171–71) and a Delamerian pegmatite from Vivonne Bay (VIV). **b** Plate tectonic reconstruction of Gondwana during the Permo-Carboniferous glaciation (glaciation maximum; Pennsylvanian–Early Permian). The base map shows the location of the continents in the supercontinent configuration at ~300 Ma[81] and the areas of ice sheet extent (with ice-flow directions)[29,39].

to capture all major provenance components[17]. In-situ dating of garnet via the U–Pb system has seen some success, but is often challenging for dating metamorphic garnets due to low uranium contents[18]. The development of laser-ablation Lu–Hf geochronology[19] provides an alternative technique to quickly date a large quantity of garnet grains with minimal sample preparation. A recent study[20] demonstrated the ability of laser-ablation Lu–Hf geochronology to date detrital garnets from a modern orogenic system (the European Alps) with a much better age recovery compared to the garnet U–Pb system in the same samples.

Here, we demonstrate that detrital garnet Lu–Hf geochronology is a feasible provenance tool for reconstructing orogenic histories at the (super) continent scale. Over 550 individual detrital garnet grains from modern beaches and Permo-Carboniferous strata in South Australia were analysed using the recently established, high-throughput laser-ablation Lu–Hf dating method[19]. The detrital garnet dates faithfully record the timing of regional orogenic events in South Australia at ~1620 and ~510 million-years ago (Ma). However, the largest detrital garnet age population in both the modern and Permo-Carboniferous sediments was dated at ~590 Ma, which together with the similar-aged dominant population of detrital zircon in the same samples, cannot be related to any known orogenic event in South

Australia. Instead, we trace this enigmatic Ediacaran population of detrital garnet and zircon to a mostly ice-covered region inboard of the Transantarctic Mountains in East Antarctica, providing new insights into the early tectonic evolution of the Pacific margin of Gondwana.

Results and discussion
Sampling and detrital garnet Lu–Hf analysis

We applied the in-situ Lu–Hf dating method to a detrital garnet provenance study of modern beach sands from the Gulf St. Vincent and Encounter Bay area in South Australia (Fig. 1a). The geology of this area preserves evidence of regional Proterozoic and early Palaeozoic orogenic events[21,22] that were integral to the assembly of the Australian continent[21,23,24]. Hence this study area is an ideal natural laboratory to test the feasibility of detrital garnet geochronology for reconstructing orogenic events from the sedimentary record. The most extensive bedrock exposures throughout the Adelaide Hills, the Fleurieu Peninsula, and Kangaroo Island (Fig. 1a) include basement rocks recording the latest Palaeoproterozoic and earliest Mesoproterozoic (ca. 1620–1600 Ma) deformation and granulite facies metamorphism associated with the Olarian Orogeny[21,25,26]. The overlying Neoproterozoic and Cambrian strata were deformed and metamorphosed

up to amphibolite facies during the Cambrian Delamerian Orogeny, which lasted from ca. 514 Ma to ca. 490–470 Ma[24,27,28]. Detrital garnet grains were separated from four modern beach sand samples and two samples of the Permo-Carboniferous glaciogenic Cape Jervis Formation (Fig. 1a; samples marked with an asterisk), the latter forming part of the Troubridge Basin that once covered large parts of southern Australia[29,30]. We also collected garnet Lu–Hf reference ages from local bedrock units, including a granulite facies metapelite from the Palaeoproterozoic Barossa Complex (sample MYPINL), a garnet–staurolite schist from the Cambrian Kanmantoo Group (Tappanappa Formation; sample 171–71), and a quartz–feldspar–muscovite–tourmaline–garnet pegmatite that intruded the Kanmantoo Group during the Delamerian Orogeny (sample VIV). Sample locations and descriptions, and mineralogical compositions are listed in Supplementary Data 1 and Supplementary Fig. 1.

The Lu–Hf isotopic analysis was conducted over 4 analytical sessions, following the methodology described in Simpson et al.[19] and detailed in the methods section. The Lu–Hf isotopic data are presented in Supplementary Data 2. Reference material Hogsbo garnet (Supplementary Fig. 2) was analysed repeatedly to correct for matrix-dependent fractionation[19,31,32] and secondary garnet reference material BP-1 (Black Point, South Australia; ref. [31,32]) was used to validate the accuracy of the Lu–Hf dates[32]. BP-1 produced garnet Lu–Hf isochron ages of 1748 ± 23 Ma, 1744 ± 19 Ma and 1749 ± 22 Ma (Supplementary Fig. 2), which are consistent with the published monazite U–Pb age of 1745 ± 14 Ma from this rock[33], underscoring the accuracy and robustness of the laser-ablation garnet Lu–Hf dating method.

Inverse isochrons, radial plots and kernel density estimate (KDE) plots for the modern beach sands, glacial sediments and local reference samples are summarised in Fig. 2 with individual plots shown in Supplementary Figs. 3–5. The single-grain dates in the KDE and radial plots were calculated as 2-point isochrons, anchored to an initial $^{177}Hf/^{176}Hf$ ratio of 3.55 ± 0.06, covering the entire range of terrestrial values[32]. For constructing KDE plots, analyses with low radiogenic Hf (resulting in imprecise single-grain dates, as shown in Fig. 2c) were filtered out of the dataset using two thresholds (cfr. ref. [20]). The detrital garnet analyses were accepted and included in the KDE plots when: (1) $^{177}Hf/^{176}Hf$ < 3, and (2) the relative uncertainty on single-grain ages <20% (see methods and Supplementary Data 2). For the beach sand samples, 32.5% of the detrital garnet analyses (132/406 grains) were accepted for the KDE plot. For the glacial strata samples of the Cape Jervis Formation, only 11% of the analyses (17/151) passed the two filters.

Detrital garnet provenance

The new garnet Lu–Hf dates from local bedrock samples are in agreement with previous estimates for the age of regional metamorphism in South Australia. Garnet porphyroblasts from a Barossa Complex gneiss (MYPINL; Supplementary Fig. 4a) yield a Lu–Hf isochron date of 1627 ± 23 Ma, agreeing with early phases of metamorphism in the complex documented by metamorphic zircon U–Pb dates of ~1632-1610 Ma[34] and monazite cores of ~1630 and ~1613 Ma[35]. They are regionally overprinted by granulite facies metamorphism at ~1590–1550 Ma, recorded by monazite U–Pb, in the Palaeoproterozoic basement inliers[25,34,35]. The garnet Lu–Hf isochron date is thus older than the bulk of the monazite dates, reflecting that the garnet Lu–Hf method records thermal history that may not be retained by monazite. Garnet porphyroblasts from an amphibolite facies metapelite within the Kanmantoo Group (171–71) and a pegmatite intruding the Kanmantoo Group (VIV) yield overlapping Lu–Hf dates of 505 ± 10 Ma and 510 ± 8.2 Ma, respectively (Supplementary Fig. 4b, c). These dates are consistent with previous estimates for the timing of metamorphism and magmatism in the Delamerian Orogeny at 515–490 Ma[27].

Detrital garnet from modern beaches and the Permo-Carbonifeous Cape Jervis Formation (CJF) yield similar age distributions in isochron, radial, and KDE plots (summarised in Fig. 2). Both groups contain minor populations of late Palaeoproterozoic-early Mesoproterozoic ages (beaches = 22%, CJF = 1%) and middle Cambrian ages (beaches = 6%, CJF = 7%), which closely overlap with the bedrock reference garnet isochron dates

for the Barossa Complex and Delamerian orogeny, respectively (Fig. 2a, b). These results clearly point to a local provenance for these garnets and demonstrate that detrital garnet geochronology faithfully records the orogenic history of the continental crust through the clastic sedimentary record.

In contrast to the minor, locally derived Proterozoic and Cambrian detrital garnet populations, the largest detrital garnet populations in both the modern beach sands (32% of all dates, 40% of filtered dates in KDE plot) and the glaciogenic Cape Jervis Formation sediments (35% of all dates, 53% of filtered dates in KDE plot) are defined at ~590 Ma and ~581 Ma, respectively. These prominent Ediacaran-aged populations cannot be linked to any known garnet-grade metamorphic event in South Australia. Notably, these age populations are beyond analytical uncertainty of the age for the onset of the Delamerian Orogeny at 514 Ma[27]. In addition, we also analysed detrital zircon grains from the modern beach sand samples (U–Pb data in Supplementary Data 3 and Supplementary Fig. 6) as a reference dataset. All samples yield essentially unimodal detrital zircon age populations at ~570 Ma, which also cannot be related to any known regional felsic magmatic event in the region. Although slightly younger than the major detrital garnet age population from the same samples, it is still likely that the ~570 Ma detrital zircons share a common source area with the detrital garnet and hence record the same tectono-metamorphic event. The zircons may, for example, record anatexis after metamorphism. Combined, the detrital garnet and zircon ages point to an ultimate sediment source in a terrane preserving an Ediacaran metamorphic and magmatic history that must lie outside of South Australia.

To aid our provenance interpretations, garnet major element compositions were acquired from the most radiogenic detrital garnets through electron probe microanalysis (see Methods section). The compositional data are provided in Supplementary Data 4 and plotted onto ternary diagrams in Fig. 3. We employed a detrital garnet classification scheme[36] (cfr. ref. [20]), which uses machine learning algorithms trained on a large database of garnet compositional data from known host rocks to predict the composition (Fig. 3a), geological setting (Fig. 3b) and metamorphic facies grade (Fig. 3c) of their host rocks. This scheme classifies the host rocks of the analysed detrital garnet grains as metamorphic rocks with mostly intermediate-felsic or metasedimentary protolith compositions. A caveat of this approach is that there is considerable overlap in the classification scheme between igneous and metamorphic garnet[37], and it is difficult to assess how the classification may be influenced by core-rim elemental fractionation when studying fragmented detrital grains. Acknowledging these limitations, the classification scheme nevertheless accurately identifies the host rocks of the locally derived Barossa and Delamerian-aged detrital garnet populations as amphibolite to granulite-grade metasedimentary rocks, which are likely to be the most abundant garnet-bearing rocks in these source areas. The predominantly metasedimentary host-rock classification of the ca. 590 Ma detrital garnet grains is, therefore, tentatively accepted as accurate (Fig. 3). Finally, we note that misclassification of igneous and metamorphic garnet would not necessarily impact our findings as most igneous garnet used in the machine learning dataset for the classification scheme[36] are from orogenic granites produced by partial melting of metasedimentary rocks and hence fundamentally reflect a similar tectonic setting to metamorphic garnet.

In identifying the source of the major ca. 590 Ma detrital garnet grains, we suggest that detrital garnet derived from modern beaches was mostly recycled from local exposures of the Permo-Carboniferous glaciogenic Cape Jervis Formation. This interpretation is consistent with the great similarity in the detrital garnet age spectra between the modern and Permo-Carboniferous samples (Fig. 2) and the absence of locally exposed ~590 Ma metamorphic source rocks (Fig. 1a). The Cape Jervis Formation was deposited in the Troubridge Basin during the late Carboniferous - early Permian when South Australia and formerly contiguous parts of Antarctica were located along the Pacific margin of East Gondwana[29,30,38]. The Cape Jervis Formation was likely deposited in association with one of several extensive ice sheets that covered large parts of Australia and Antarctica as Gondwana moved over the South
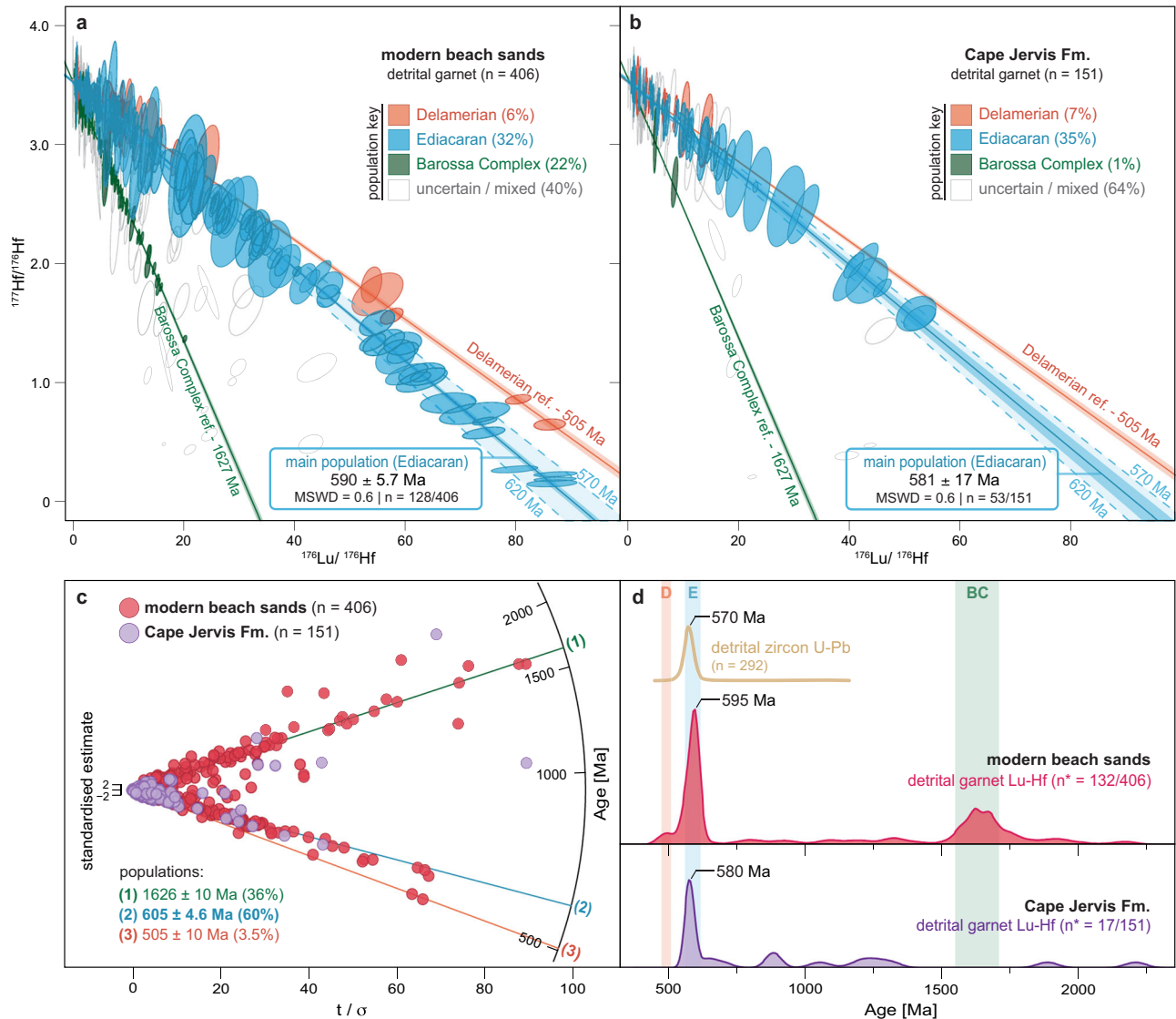
Fig. 2 | Detrital garnet Lu–Hf geochronology. a Combined inverse Lu–Hf isochron plot for all analysed modern beach samples from South Australia (PCB, PMB, PVB and MYB; see Fig. 1a for sample locations). **b** Combined inverse Lu–Hf isochron plot for the two samples from the glaciogenic Cape Jervis Formation (BQ7 and BS2). Reference Lu–Hf isochrons for the regional Barossa Complex (green isochron line) and Delamerian Orogeny (red isochron line) metamorphism were calculated based on analyses for the Myponga Inlier gneiss (sample MYPINL; ~1627 Ma; Supplementary Fig. 4a) and Kanmantoo Group metapelite (sample 171–71; ~505 Ma; Supplementary Fig. 4b), respectively. The detrital garnet ellipses in **a** and **b** represent single-grain data points with 2σ uncertainty. The ellipses were colour-coded according to their interpreted source in South Australia (Delamerian in red, Ediacaran in blue, Barossa Complex in green). The main detrital garnet population is Ediacaran in both the modern beach sand and Permo-Carboniferous glacial strata samples, suggesting that Ediacaran garnets in the modern beach sands were recycled from the Cape Jervis Formation before deposition. **c** Radial plot of single-grain garnet dates (modern beach sand data in red, Cape Jervis Formation data in purple),

plotted against their precision as calculated by IsoplotR[75]. The most radiogenic garnet grains (^{177}Hf/^{176}Hf < 1.5) produce the most precise Lu–Hf ages (as illustrated in Supplementary Fig. 5), adding more weight to garnet population identifications. **d** Kernel density estimate (KDE) plots of single-grain garnet dates (modern beach sand data in red, Cape Jervis Formation data in purple), compared to zircon dates (in yellow) from the same samples. The single-grain dates were calculated as 2-point isochrons and low-radiogenic garnets were filtered out using the following criteria: (1) ^{177}Hf/^{176}Hf < 3, and (2) the relative uncertainty on single-grain ages <20%. n^* indicates the number of grains that remain after the application of these two filters. For the zircon U–Pb KDE plot, detrital zircon single-grain ages with discordance > ±5% were rejected. The detrital garnet Lu–Hf isotopic data was plotted using IsoplotR[75], and this figure shows how each plot (isochron, KDE and radial) is able to detect the three distinct detrital garnet populations (Palaeo-Mesoproterozoic in green, Ediacaran in blue and Cambrian in red). The individual isochron and KDE plots for each detrital garnet sample can be found in Supplementary Fig. 3.

Pole (Fig. 1b)[38–40]. Ice-flow indicators within the Cape Jervis Formation, including striations, erosional troughs and chatter marks, consistently record ice-flow from the southeast to northwest[29,30,38,41,42], suggesting a sediment source in East Antarctica within reconstructed Gondwana (Figs. 1b and 4a). Ice-flow indicators from time-equivalent strata elsewhere in southeastern Australia and East Antarctica are consistent with a contiguous ice sheet centred on a palaeo-high inboard of the present-day George V Land and Transantarctic Mountains (Fig. 1b)[39]. Therefore,

we suggest the abundant ca. 590 Ma detrital garnet grains found along the coast of southern Australia were ultimately derived from an Ediacaran terrane currently located within the largely ice-covered interior of East Antarctica inboard of George V Land and the Transantarctic Mountains (Figs. 1b and 4a). Notably, this ice catchment is not connected to other reconstructed Permian ice catchments in East Antarctica that could have sampled other Ediacaran Orogens such as those exposed in Dronning Maud Land or Prydz Bay (Fig. 1b).
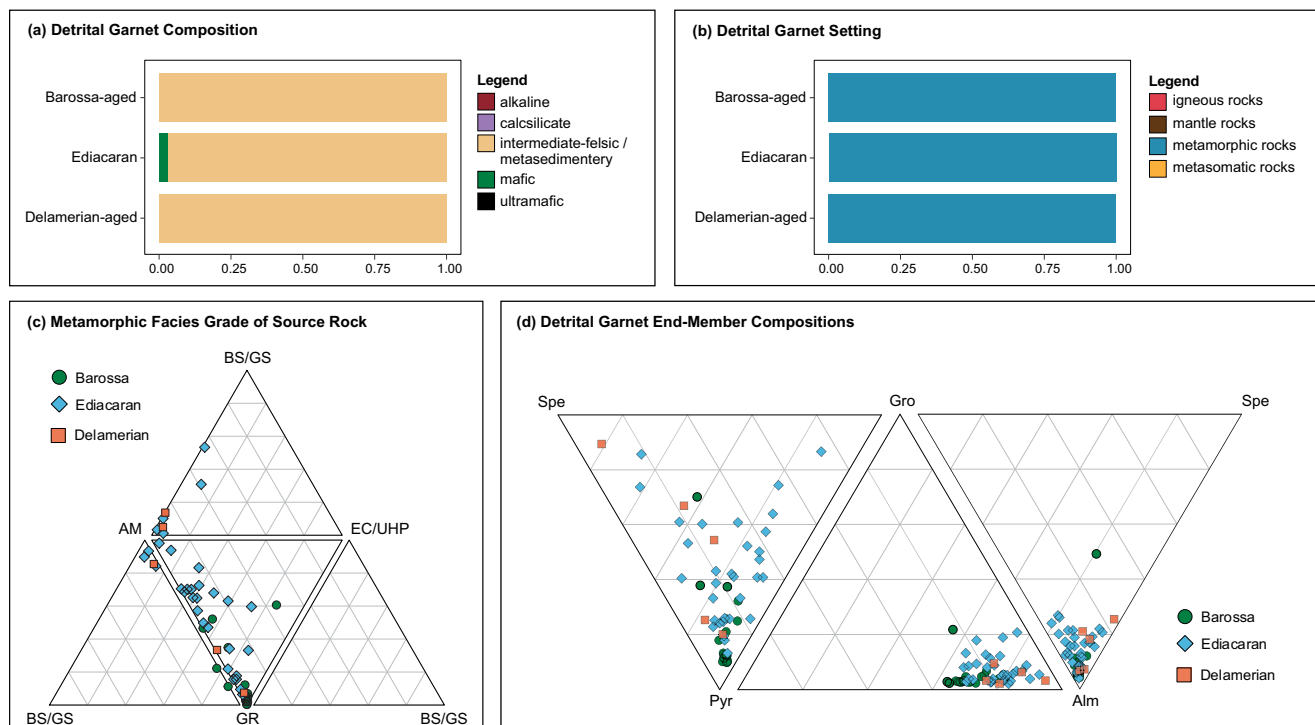
Fig. 3 | Detrital garnet EPMA compositional data for the beach sand samples MYB, PCB, PMB and PVB. a, b Detrital garnets are classified according to the interpreted composition and setting of their host rocks, respectively, using the scheme of Schönig et al.[36]. **c** Detrital garnets plotted on a ternary diagram by metamorphic facies grade, using the same classifier[36] (cfr.[20]). **d** Combined triple ternary plot[82], which displays the detrital garnets based on their end-member compositions. The detrital garnets are all grouped or colour-coded according to their interpreted source in South Australia (Palaeo-Mesoproterozoic Barossa Complex as green circles, Ediacaran as blue diamonds, Delamerian as red squares). The EPMA compositional data is provided in Supplementary Data 4. AM amphibolite facies grade, BS/GS blueschist/greenschist facies grade, EC/UHP eclogite/ultrahigh-pressure facies grade, GR granulite facies grade, Alm almandine, Gro grossular, Pyr pyrope, Spe spessartine.

## Initiation of the palaeo-Pacific convergent margin of Antarctica

The Transantarctic Mountains (TAM) provide the most extensive exposures of the Ediacaran–Cambrian Ross Orogen[43]. This orogen is considered to record an Andean-type convergent system along the palaeo-Pacific margin of Gondwana. The orogen records a complex tectonic history involving oblique convergence punctuated by episodes of extension with the bulk of arc magmatism, high-temperature metamorphism, and deformation occurring between ca. 520 and 480 Ma[43–45]. Although the Andean-type tectonic setting of the Ross orogen is well established[43], the timing of subduction initiation and the onset of convergence are poorly resolved.

Outcrop evidence brackets the onset of the Ross orogenic cycle to sometime between the formation of the rifted continental margin at ca. 670—650 Ma[46–48] and the oldest exposed calc-alkaline plutons (in the Central TAM) at ca. 550 Ma[44,49]. Evidence for pre-550 Ma magmatism comes from common ca. 590–570 Ma zircon U–Pb ages in late Neoproterozoic-early Palaeozoic strata along the TAM, which are interpreted to be sourced from the incipient Ross continental arc[43,44,50–52]. Additional evidence for ca. 570–590 Ma felsic magmatism along the Ross orogen includes a granitoid clast from the Nimrod Glacier, which yields a complex distribution of U–Pb zircon ages between ca. 590 Ma and ca. 560 Ma but does not have a distinct calc-alkaline geochemical signature[44]. A ca. 584 Ma granitoid dredged from offshore George V Land[50] may also record the same magmatic event. Although ca. 590–570 Ma felsic magmatism along the Ross orogen appears to be regionally extensive, a direct link with the onset of convergent margin tectonism is hindered by the paucity of diagnostic geochemical signatures in detritus derived from this magmatic province and the sparse record of contemporaneous metamorphism and deformation in the exposed geology of the TAM.

Early work in the central TAM attributed the deformation of the Neoproterozoic Beardmore Group to a pre-Ross, Ediacaran orogenic event termed the Beardmore Orogeny[53]. However, subsequent revisions to the stratigraphy of this area, coupled with Ar–Ar and U–Pb dates, demonstrate that the apparently earlier episode of metamorphism and deformation is instead an expression of the main Cambrian Ross orogenic pulse, leading to the abandonment of the Beardmore Orogeny[54,55]. More recently, outcrop evidence for Ediacaran metamorphism and deformation in the Transantarctic Mountains has been re-established in the Skelton Glacier region of Southern Victoria Land (Fig. 4a, Supplementary Fig. 7). Here, amphibolite facies metasedimentary and minor meta-igneous rocks record contractional deformation and a Barrovian metamorphic history dated via U–Pb monazite and solution-based Lu–Hf whole rock-garnet isochrons to ~590–570 Ma with individual dates as old as ~615 Ma[56].

Our new detrital garnet data greatly expands the geochronological evidence for Ediacaran metamorphism along the Antarctic segment of the palaeo-Pacific margin of Gondwana. Palaeo-ice sheet reconstructions based on the distribution of Permian-Carboniferous glacial deposits suggest that deposition in the Troubridge Basin occurred along the northern extent of an approximately 1000 × 2000 km ice sheet that was centred on a palaeo-highland inboard of the present-day TAM and covered most of the eastern margins of East Antarctica and southern Australia within reconstructed Gondwana (Fig. 1b)[39,40]. The presence of abundant ~590 Ma detrital metamorphic garnet grains (Fig. 2 and Fig. 3) in sediments eroded from this continental-scale catchment argues for a source in a regional-scale ~590 Ma metamorphic province (Fig. 4). Ediacaran garnet-grade metamorphic events have not been recorded in the basement of southern Australia, and hence it is unlikely that this metamorphic province extended into the Australian continent. Glacial erratics yielding ca. 580–570 Ma metamorphic ages dredged offshore from the Mertz Glacier suggest a northern extent in subglacial George V Land[50] (Fig. 4a). The southern extent of the province may have been sampled by the ca. 590 Ma granitoid clast from the Nimrod
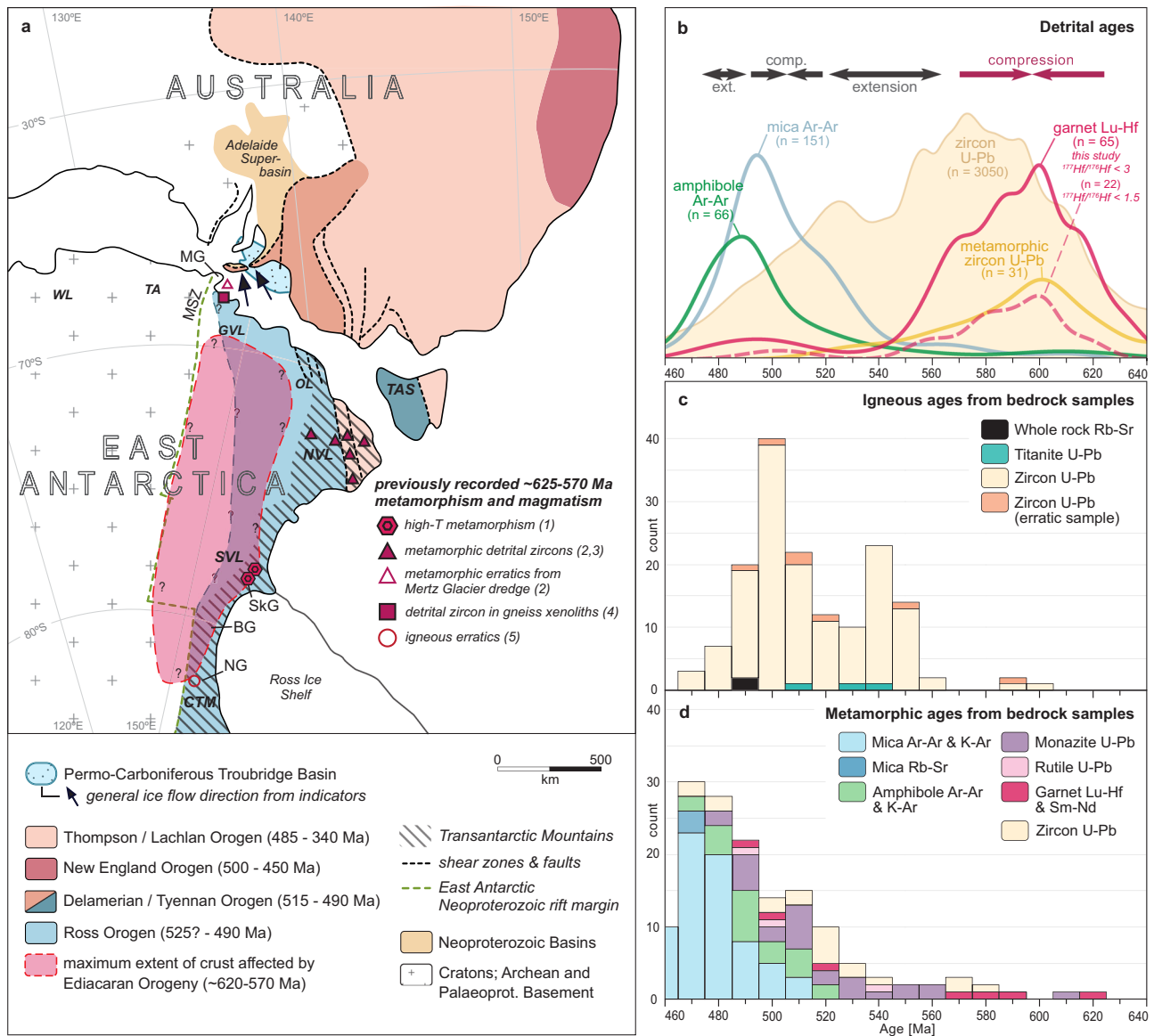
Fig. 4 | Configuration of short-lived orogenic systems in eastern Gondwana, with compiled datasets of Ediacaran–Cambrian dates. a Simplified tectonic map of Australia and Antarctica in the early Permian, showing the extent of the major early Palaeozoic (Cambrian-Ordovician) orogenic systems. Ediacaran-age (~620–570 Ma) metamorphic and magmatic records from recent studies of samples from the Trans-antarctic mountains and clasts from Mertz Glacier dredge are as plotted[43] and include (1) metamorphic garnet[56], (2) metamorphic zircon[50], (3) metamorphic erratic[51], (4) detrital zircon[52] and (5) igneous erratic[44] data. The base map in **a** is adapted from Lawver et al.[81], and the main geological units and tectonic structures[30,43,83–87] are plotted together with the present-day coordinates of Australia and Antarctica. BG Beardmore Glacier, CTM Central Transantarctic Mountains, MG Mertz Glacier, MSZ Mertz Shear Zone, NG Nimrod Glacier, NVL Northern Victoria Land, OL Oates Land, SkG Skelton Glacier, SVL Southern Victoria Land, TA Terre Adélie, TAS Tasmania, WL Wilkes Land. **b** Detrital, **c** igneous and **d** metamorphic age profiles derived from previous studies along the coast of East Antarctica (between 140°E and 175°E) and the Transantarctic Mountains. Detrital ages for glaciomarine sediments in the Ross Sea are also included. References are listed in Supplementary Table 1, and the compiled ages are plotted per region in East Antarctica in Supplementary Fig. 7. The detrital garnet Lu–Hf ages (pink KDE) in (**b**) are from this study and were added for comparison with the existing data from other detrital minerals (KDE in full line; grains with $^{177}Hf/^{176}Hf < 3$ and relative uncertainty on single-grain ages <20%). The dashed line KDE only includes the garnets with $^{177}Hf/^{176}Hf < 1.5$, and illustrates the same Ediacaran peak is present when only the most precise garnet dates are plotted. Detrital garnet Lu–Hf and detrital metamorphic zircon U–Pb ages are consistently older than the igneous and unclassified detrital zircon U–Pb ages. The mica and amphibole Ar–Ar cooling ages clearly reflect the timing of Cambrian Ross Orogeny metamorphism, a phase that is distinctly younger than the Ediacaran detrital garnet and metamorphic detrital zircon peaks. The periods of alternating compression and extension[43] were based on changes in syn-tectonic magma compositions and field structures. An early phase of Ediacaran thickening, as derived from the new detrital garnet ages in this study, is indicated with pink arrows. The dates for bedrock samples in **c** and **d** clearly represent Ross Orogeny metamorphism but are almost completely devoid of Ediacaran ages. Based on observations from available bedrock exposures of Ediacaran metamorphism and magmatism in (**a**) and palaeo ice-flow directions in Fig. 1b (and see also main text), we propose a rough estimate for the maximum extent of the crust affected by Ediacaran thickening (red area), stretching between inland George V Land and inboard the Transantarctic Mountains.

Glacier[44]. We suggest that the Ediacaran garnet-bearing rocks of the Skelton Group in Southern Victoria Land[56] are exposures of this regionally extensive Ediacaran metamorphic province (Fig. 4a). If the Barrovian metamorphic rocks exposed in Skelton Glacier are representative of the larger sub-glacial source region sampled by detrital garnet in South Australia, our findings support the presence of a regionally extensive area inboard of the TAM that experienced Ediacaran crustal thickening. We suggest that crustal thickening in this sub-glacial province documents the first pulse of convergent margin tectonics associated with the Ross orogenic cycle, based on the Ediacaran timing of metamorphism and magmatism and its position

inboard of the predominantly Cambrian metamorphism and deformation preserved in the TAM.

The tectonic history of the Ross orogeny is generally interpreted in the context of alternating episodes of compression (or transpression) and extension in response to changing plate kinematics and possibly terrane accretion[44,56,57]. Although along-strike variations in the magmatic, metamorphic, and structural history of the Ross orogen argue against a simple accordion-style tectonic evolution[43], the general cyclical nature of convergence and extension associated with long-term continent-dipping subduction is supported by our interpretation of regional Ediacaran crustal thickening inboard of the TAM. Compiled igneous and metamorphic ages from the TAM show that early crustal thickening at ca. 590–570 Ma is temporally separated from the dominant phase of ca. 520–490 Ma contractional tectonism by an episode of crustal extension marked by ca. 565–525 Ma alkaline, carbonatitic, and mafic subalkaline magmatic activity in Southern Victoria Land (Fig. 4b–d)[58,59]. The refined temporal framework for the Ross orogeny presented in Fig. 4 reinforces an orogenic cyclicity, characterised by short-lived contractional events, each lasting about 30–40 Myrs, separated by 40–50 Myrs of extension[43].

Although a detailed regional synthesis is beyond the scope of this paper, the Ross orogen is generally interpreted to record the first cycle of convergence along the palaeo-Pacific margin of Gondwana as a part of the larger Terra Australis orogen[60]. Most Gondwana reconstructions correlate the Ross orogen with the Delamerian orogen of southern Australia, with both regions recording contractional deformation, metamorphism, and convergent margin magmatism at ca. 520–480 Ma[24,61]. However, this study highlights potentially substantial differences in the early tectonic history of the Palaeo-Pacific margin of Gondwana in East Antarctica compared to southern Australia. Specifically, the episode of crustal thickening along the East Antarctic segment of the margin at ca. 590–570 Ma inferred from our new detrital garnet data contrasts with the tectonic setting of southern Australia at this time, which records continental rifting at ca. 580 Ma and subsequent passive margin sedimentation[23,62]. Therefore, contemporaneous Ediacaran convergence in East Antarctica and extension in southern Australia should be considered in tectonic models for the evolution of the palaeo-Pacific margin of Gondwana (e.g., ref. 61). A detailed understanding of the tectonic character, spatial extent, and regional significance of the inferred Ediacaran phase of crustal thickening in the Ross orogen is ultimately precluded by the extensive cover of the polar ice-cap. Nevertheless, this study highlights the potential of detrital garnet to reconstruct orogenic histories from the clastic sedimentary record to provide first-order constraints on the tectonic evolution of poorly exposed or inaccessible areas of the continental crust.

Methods
Sample descriptions and sample imaging
Detrital garnets from four modern beach sand samples (MYB, PCB, PMB and PVB) and two glacial strata samples from the Permo-Carboniferous Cape Jervis Formation in Kangaroo Island (BS2 and BQ7) were analysed. For each of the modern beach sand samples, between ~200 and 500 g of garnet sand was collected. Detrital garnets were abundant (~50–80%) in the heavy mineral fractions, and hence no further separation steps were needed. A single layer of minerals was mounted in 2.5 cm round epoxy resin and polished using standard techniques to expose the internal mineral surfaces for imaging. Heavy mineral separates of the Cape Jervis Formation samples BS2 and BQ7 were provided by the South Australia Drill Core Reference Library, Department for Energy and Mining (South Australia). The heavy mineral separates (38 μm–1 mm) were separated by the previous workers[63] and were mounted in epoxy resin for this study. The three bedrock samples from South Australia (Barossa Complex gneiss, Delamerian schist and Delamerian pegmatite) were cut into small ~1 × 1 cm rock blocks, mounted in 2.5 cm round epoxy resin and then polished using standard techniques to expose the garnet porphyroblasts for laser-ablation analysis.

Prior to laser-ablation garnet Lu–Hf analysis, the sample mounts of the four modern beach sand samples (MYB, PCB, PMB and PVB) were scanned using a Hitachi SU3800 automated mineralogy scanning electron microscope (SEM) at Adelaide Microscopy, the University of Adelaide. Mineral Liberation Analysis (MLA) maps were collected to assess which heavy minerals are present in each placer sand sample and to estimate their heavy mineral and grain size distributions. Pie charts of the heavy mineral distributions are provided in Supplementary Fig. 1. Garnet is the most abundant heavy mineral in each modern beach sand sample (50–75 volume %). Other common heavy minerals are epidote, rutile, zircon, and Fe-oxides. Using the SEM-MLA maps, detrital garnets were selected for Lu–Hf analysis. Additionally, backscattered electrons were used to examine the selected detrital garnets for zonation patterns. The detrital garnets from the modern beach sand samples are mostly subangular-subrounded, vary in colour from colourless to dark orange–pink and have grain sizes between 50 μm and 1 mm. Ref. 63 previously described the heavy mineral distributions of the Permo-Carboniferous glacial strata samples BS2 and BQ7 from the Cape Jervis Formation. The distributions are also plotted as pie charts in Supplementary Fig. 1. Similar to the modern beach samples, the heavy mineral fractions of the glacial strata mostly contain garnet (60–80 volume %). The detrital garnets vary in colour from colourless to orange–pink and are mostly subangular-subrounded.

Using the SEM-MLA maps, detrital zircons were selected for U–Pb geochronology. The Myponga Beach placer sand sample (MYB) and the Cape Jervis Formation heavy mineral separates (BS2, BQ7) did not have enough suitable zircons for a representative detrital zircon U–Pb analysis. Detrital zircon U–Pb ages were therefore only obtained from samples PCB, PMB and PVB (see further). The detrital zircons are 35–250 μm and subangular-subrounded. Cathodoluminescence (CL) images were collected for the selected detrital zircons and primarily revealed magmatic growth for most of them. In detrital zircons with a distinct core and rim (<5% of all zircons), the rims were targeted for U–Pb geochronology.

Sample locations and descriptions for the detrital garnet (MYB, PCB, PMB, PVB, BS2 and BQ7) and basement samples (MYPINL, 171–71 and VIV) are provided in Supplementary Data 1.

(Detrital) garnet laser ablation ICP–MS/MS Lu–Hf Geochronology
The Lu–Hf laser ablation tandem inductively coupled mass spectrometry (LA–ICP–MS/MS) analysis undertaken in this study follows the method as established and described by Simpson et al.[19] and other recent work[20,31,64,65]. The garnet Lu–Hf isotopic data were collected across four laser sessions, using a RESOlution 193 nm excimer laser unit attached to an Agilent 8900 QQQ mass spectrometer (ICP–MS/MS) at Adelaide Microscopy, the University of Adelaide. The Lu–Hf results are provided in Supplementary Data 2. Detrital garnets from the modern beach sand samples (MYB, PCB, PMB and PVB) were analysed in session 1, detrital garnets from the Cape Jervis Formation samples (BQ7, BS2) were analysed in session 2, garnet porphyroblasts from the Barossa Complex gneiss (MYPINL) were analysed in session 3, and the Delamerian basement samples (171–71 and VIV) were analysed in session 4.

Laser beam diameters of 120 μm and 173 μm were used for laser ablation, depending on the grain size of the (detrital) garnet. Each individual analysis includes 40 s of ablation time and 30 s of background measurement, with a repetition rate of 10 Hz and fluence of approximately 3.5 J cm^{-2}. A reaction gas of 10% NH_3 in 90% He was introduced to the collision cell at a total flow rate of 3 mL min^{-1} to promote high-order reaction products of Hf, while equivalent Lu and Yb reaction products were negligible. The mass-shifted (+ 82 amu) reaction products of $^{176+82}Hf$ and $^{178+82}Hf$ reached the highest sensitivity of the measurable range and were analysed free from isobaric interferences. ^{175}Lu and ^{178}Hf were used as a proxy for the calculation of ^{176}Lu and ^{177}Hf, respectively; for a detailed description of this process, see ref. 19. The following isotopes were also measured to monitor the presence of mineral inclusions in the analysed garnets: ^{24}Mg, ^{27}Al, ^{43}Ca, ^{47}Ti, ^{57}Fe, ^{89}Y, ^{90}Zr, ^{140}Ce and ^{172}Yb.

Synthetic glass standard NIST-610 (with $^{176}Lu/^{177}Hf = 0.1379 \pm 0.005$ and $^{176}Hf/^{177}Hf = 0.2821 \pm 0.000009$[66,67]) was used as primary reference material, and analysed with a spot size of 43 μm. The LADR software

package[68] was used for Lu–Hf data processing and reduction, to correct for instrumental mass bias and drift against NIST-610. As demonstrated by ref. 19, downhole fractionation is not observed, and thus laser beam diameters can be chosen specific to the sample of interest to maximise sensitivity. NIST-610 was also used (with Al as the internal standard element) to calculate the concentrations of the analysed trace elements in LADR[68]. A total of 652 detrital garnets were analysed in this study, of which 95 analyses were omitted due to contamination from inclusions or poor signal intensities. In more detail, we removed all analyses with unstable time signals (in particular, the 175Lu signal), with low count rates (<10 000 CPS), when the epoxy was ablated instead of a garnet grain and when inclusions were co-ablated. Inclusions were monitored by looking at spikes in the concentrations (>500 ppm) of Sr, Ti, Zr, and Ce to detect the presence of apatite, rutile, zircon and monazite, respectively. To filter for potential contamination by xenotime, analyses with both Y and Yb concentrations exceeding two standard deviations from the median value for all analysed garnets were also excluded (cfr.[69]). Afterwards, 406 detrital garnet analyses remained for the beach sand samples and 151 for the glacial strata samples of the Cape Jervis Fm, which were all included in the isochron and radial plots. For the construction of the Kernel Density Estimate (KDE) plots, two additional filters were applied to the remaining 557 detrital garnet analyses (see further).

Reference material Hogsbo garnet was analysed repeatedly to correct for matrix-dependent fractionation[19,31,32]. Hogsbo garnet has a published columbite U–Pb age of 1029 ± 1.7 Ma[70] that is used as the reference age for Lu–Hf ratio corrections[32]. The Lu–Hf isotopic results for Hogsbo in this study are given in Supplementary Data 2 and plotted in Supplementary Fig. 2 and are consistent with previous studies[19,31,32,64,65]. To account for the observed session-specific age offset, a correction was applied to the ^{176}Lu/^{177}Hf ratios of all unknowns based on the measured versus observed Lu–Hf ratio intercept for Hogsbo. The correction factors and calculations are given in Supplementary Data 2. The accuracy of the Lu–Hf ages after the correction was validated by repeated analyses of secondary garnet reference material BP-1 (Black Point, South Australia;[31,32]) producing garnet Lu–Hf isochron ages (corrected against Hogbso; Supplementary Data 2, Supplementary Fig. 2) of 1748 ± 23 Ma, 1744 ± 19 Ma and 1749 ± 22 Ma that are consistent with a previously published monazite U–Pb age of 1745 ± 14 Ma[33].

The garnet Lu–Hf isotope ratios are visualised using inverse isochrons, following ref. 71. The inverse Lu–Hf isochron plots are anchored against an initial ^{177}Hf/^{176}Hf ratio of 3.55 ± 0.06 (cfr.[11,72]). This assumed initial Hf composition spans the entire range of initial ^{177}Hf/^{176}Hf ratios of the terrestrial reservoir (e.g.[73,74]) and does not significantly impact the resulting Lu–Hf isochron ages (in contrast to initial Pb or Sr compositions for the U–Th–Pb and Rb–Sr systems[19]).

The Lu–Hf isochron plots and ages were calculated using IsoplotR[75], and data point ellipses are 2σ uncertainty. For the detrital garnet samples (modern beach sands and Permo-Carboniferous strata), the individual Lu–Hf isochrons are provided in Supplementary Fig. 3a–f. These isochrons show that the Ediacaran ~620–570 Ma signal (see main text, Fig. 2 and Supplementary Fig. 3) is present in each analysed detrital garnet sample. The Lu–Hf isochron ages of the analysed Barossa Complex gneiss (sample MYPINL; ~1627 Ma; Supplementary Fig. 4a) and Kanmantoo Group metapelite (sample 171–71; ~505 Ma; Supplementary Fig. 4b) were used as reference ages for Palaeo-Mesoproterozoic Barossa Complex and Cambrian Delamerian Orogeny metamorphism, respectively. Using these reference ages, the single-grain dates of the detrital garnets were classified according to their interpreted source in South Australia (Delamerian, Ediacaran or Palaeo-Mesoproterozoic Barossa Complex). The ellipses included in the three population isochrons (blue isochrons; Fig. 2a, b; Supplementary Fig. 3) were selected based on the obtained single-grain Lu–Hf dates, the isochron MSWD values and the mathematically calculated peak-fitted age distributions of their radial plots.

Radial plots visualise dates against precision. Here (Fig. 2c; Supplementary Fig. 5), the single-grain garnet dates are plotted in IsoplotR as 2-point isochron dates versus their fully propagated uncertainties[75].

Supplementary Fig. 5 colour-codes the single-grain dates based on the ^{177}Hf/^{176}Hf ratio of each analysis and illustrates that the most radiogenic garnet grains (^{177}Hf/^{176}Hf < 1.5) produce the most precise Lu–Hf dates. During data processing, peak-fitted age distributions were also calculated for each individual detrital garnet sample. The peak-fitted ages of the Ediacaran populations varied between 620 and 570 Ma (30-45% of the analysed detrital garnets) for each sample. This observation was used for the calculation of the average main population isochrons (blue isochrons) in Fig. 2 and Supplementary Fig. 3. Garnets with single-grain ages between 620 and 570 Ma (blue ellipses) were included in the calculation of the population isochrons, garnets with single-grain ages > 620 Ma or <570 Ma (grey single-grain ellipses) were omitted from the calculation. The resulting population isochrons (blue isochrons) have MSWD values between 0.2 and 1.1 for each individual sample (Supplementary Fig. 3a–f), conforming with statistically single populations[76]. Additionally, when plotting the modern beach sand samples and Permo-Carboniferous glacial strata samples together (Fig. 2a, b), the resulting population isochrons also have MSWD values that conform with statistically single populations[76].

KDE plots were calculated in IsoplotR (Fig. 2d, Supplementary Fig. 3g). As for the radial plot, the ages in a KDE plot are single-grain dates calculated as 2-point isochrons. Detrital garnets with a high ^{177}Hf/^{176}Hf ratio will plot closer to the isochron anchor and will, therefore, have a less reliable (low precision) single-grain isochron age (as illustrated in the radial plot of Supplementary Fig. 5), causing unwanted scatter in the KDE plots. To account for this, the less precise garnet Lu–Hf single-grain ages were first filtered out of the dataset. Here, singe-grain dates based on measurements with ^{177}Hf/^{176}Hf < 2 and relative age uncertainty <20% were accepted, and all other detrital garnets single-grain ages were rejected (cfr.[20]). The percentage of detrital garnets that were omitted to construct the KDE plot is given in Supplementary Data 2 for each sample. For the beach sand samples and glacial strata samples, 32.5% (132/406 grains) and 11% of the analyses (17/151) of the analysed detrital garnet analyses were accepted for the KDE plot, respectively. The KDE plots in Fig. 2d (Lu–Hf data in red) define a main detrital garnet population at ~595 Ma for the modern beach sand samples and at ~580 Ma for the Permo-Carboniferous glacial strata. These ages are in agreement with the calculated Lu–Hf isochron ages (Fig. 2a, b).

The older detrital garnets (Fig. 2 and Supplementary Fig. 3; grey ellipses with ages >620 Ma and not assigned to Barossa Complex metamorphism) gave Lu–Hf isochrons with MSWD > 1, were not mathematically classified as separate age distributions by IsoplotR[75] in the radial plots and are not expressed in the KDE plots. This is most likely due to the limited number of garnets with a single-grain age >620 Ma and due to their high ^{177}Hf/^{176}Hf ratios (low precision). Hence, these detrital garnets could not be assigned to distinct detrital garnet populations.

The Lu–Hf isochrons of the analysed basement samples from South Australia are provided in Supplementary Fig. 4. Migmatitic Barossa Complex (Myponga Inlier) sample MYPINL has a metamorphic Lu–Hf isochron age of 1627 ± 23 Ma (Supplementary Fig. 4a). The Delamerian samples 171–71 and VIV have Lu–Hf isochron ages of 505 ± 18 Ma and 510 ± 8.2 Ma, respectively (Supplementary Fig. 4b, c).

Detrital zircon laser ablation ICP–MS/MS U–Pb Geochronology

Laser ablation ICP–MS U–Pb geochronology was conducted on detrital zircons from placer sand samples PCB, PMB and PVB (the three samples with sufficient detrital zircons for analysis) across two laser sessions, using a RESOlution LR 193 nm Excimer laser unit attached to an Agilent 8900 mass spectrometer (ICP–MS/MS) at Adelaide Microscopy, the University of Adelaide. Using the same sample mounts as for the garnet Lu–Hf analysis, detrital zircons were selected using the SEM-MLA maps and zircon CL images (see earlier). Zircon grains are between 35 and 250 μm and were targeted with a laser beam size of 30 μm. The analyses included 30 s of laser ablation and 30 s of background measurement and were conducted with a repetition rate of 5 Hz and a fluence of 2.12 J cm^{-2}. The zircon U–Pb isotopic results are provided in Supplementary Data 3.

Data reduction was performed using LADR[68], and primary zircon standard GJ-1 was used for elemental fractionation and mass bias corrections. Primary reference material GJ-1 zircon has a recommended TIMS $^{206}Pb/^{238}U$ age of 601.86 ± 0.37 Ma[77] and gave consistent calculated weighted mean ages for both sessions (Supplementary Data 3). The accuracy of the U–Pb isotopic results was examined with two secondary reference materials: Plešovice zircon ($^{206}Pb/^{238}U$ age of 337.13 ± 0.37 Ma;[78]) and 91500 (zircon $^{206}Pb/^{238}U$ age of 1063.51 ± 0.39 Ma;[77]). The calculated weighted mean ages for Plešovice and 91500 zircon were within the uncertainty of the published ages for both laser ablation sessions (Supplementary Data 3). Zircon trace element concentrations were calculated in LADR against synthetic glass standard NIST-610[67]. For the isotopic and trace element data reduction, an approximate concentration of 15.32 wt% Si was used as the internal standard. The trace element concentrations were used to check for failed zircon analyses during time signal processing in LADR. Zircons with failed analyses (e.g., due to fractures or complete removal of the zircon grain) or inclusions (that were not detected in the CL images) were omitted from the dataset. Out of 337 zircon U–Pb analyses, 10 were omitted during time signal processing in LADR.

For the Kernel Density Estimate (KDE) plots (Fig. 2d, Supplementary Fig. 6), detrital zircons with discordance > ± 5 % were rejected (Supplementary Data 3). In total, 10% of detrital zircons (34 out of 327 analyses) were rejected. For detrital zircons < 1 Ga, $^{206}Pb/^{238}U$ ages are reported and included in the KDE plots. For zircons > 1 Ga, $^{207}Pb/^{206}Pb$ ages are used. The KDE plots were calculated in IsoplotR[75] and defined a mean detrital zircon age population at ~570 Ma for the modern beach sand samples (Fig. 2d).

(Detrital) garnet major element electron probe microanalysis

To examine whether a correlation exists between detrital garnet end-member composition and detrital garnet Lu–Hf age, (detrital) garnet major element compositions were acquired and quantified using a CAMECA SXFive electron probe microanalyser (EPMA) with five wavelength-dispersive spectrometers (WDS) at Adelaide Microscopy, the University of Adelaide. A beam current of 20 nA with a beam diameter of 5 μm and an accelerating voltage of 15 kV was used for spot analysis. Both synthetic and natural-certified standards were analysed for data calibration procedures. The data calibration and reduction were performed in Probe for EPMA, a software package distributed by Probe Software Inc. Compositional data was obtained for the most radiogenic detrital garnet grains ($^{177}Hf/^{176}Hf < 2.5$). The representative EPMA major element chemistry is provided in Supplementary Data 4, and the accompanying plots can be found in Fig. 3 and Supplementary Fig. 8. Note that only the analyses with a total wt% between 99% and 101% were accepted, the analyses with a total wt% outside of this range were rejected from the dataset.

A first EPMA session was conducted to compare the end-member compositions of the detrital garnets from the Myponga Beach placer sand (MYB, Supplementary Fig. 9) with garnet porphyroblasts from the local Barossa Complex basement rocks (Myponga Inlier, MYPINL) for the Myponga Beach case study (Supplementary Note 1). Only the most radiogenic detrital garnets from the MYB placer sand ($^{177}Hf/^{176}Hf < 2.5$), were analysed here (Supplementary Data 4). The detrital garnet end-member compositions were afterwards plotted on a ternary diagram for visualisation (Supplementary Fig. 8a). For the garnet porphyroblasts from local basement sample MYPINL, transect profiles were obtained across two representative garnets (Supplementary Data 4). No distinct zoning patterns were found along the two garnet porphyroblast transects (Supplementary Fig. 8c). The EPMA data reveals a compositional link between the Palaeoproterozoic detrital garnets of Myponga Beach (~1626 Ma; Supplementary Fig. 3a, population MYB(2)) and the garnet porphyroblasts from the Barossa Complex (~1627 Ma; Supplementary Fig. 4a) when they are plotted together on a ternary diagram (Supplementary Fig. 9d).

During the second EPMA session, the most radiogenic detrital garnets ($^{177}Hf/^{176}Hf < 2$) from the other three placer sand samples (PCB, PMB and PVB) were analysed to examine whether a correlation exists between detrital garnet end-member composition and detrital garnet Lu–Hf age. All data was plotted on a ternary diagram (Supplementary Fig. 8b), but no compositional link seems to be present between garnets from the same age population. The detrital garnets have slight variations in their end-member compositions, regardless of their single-grain age.

Data availability

The data used and produced in this study are provided in Supplementary Data 1–4: sample locations and descriptions (Supplementary Data 1), garnet Lu–Hf data (Supplementary Data 2), zircon U–Pb data (Supplementary Data 3), representative EPMA major element analysis (Supplementary Data 4). The dataset, including the Supplementary Notes, Supplementary Figs. and Supplementary Table 1, is also available in the accompanying Figshare repository.

References

1. Cawood, P. A., Hawkesworth, C. J. & Dhuime, B. Detrital zircon record and tectonic setting. *Geology* **40**, 875–878 (2012).
2. Moecher, D. P. & Samson, S. D. Differential zircon fertility of source terranes and natural bias in the detrital zircon record: Implications for sedimentary provenance analysis. *Earth Planet. Sci. Lett.* **247**, 252–266 (2006).
3. O'Sullivan, G. J., Chew, D. M. & Samson, S. D. Detecting magma-poor orogens in the detrital record. *Geology* **44**, 871–874 (2016).
4. Hawkesworth, C., Cawood, P., Kemp, T., Storey, C. & Dhuime, B. A matter of preservation. *Science* **323**, 49–50 (2009).
5. Hietpas, J., Samson, S., Moecher, D. & Schmitt, A. K. Recovering tectonic events from the sedimentary record: Detrital monazite plays in high fidelity. *Geology* **38**, 167–170 (2010).
6. Pereira, I., Storey, C. D., Strachan, R. A., Bento Dos Santos, T. & Darling, J. R. Detrital rutile ages can deduce the tectonic setting of sedimentary basins. *Earth Planet. Sci. Lett.* **537**, 116193 (2020).
7. Baxter, E. F., Caddick, M. J. & Dragovic, B. Garnet: a rock-forming mineral petrochronometer. *Rev. Mineral. Geochem.* **83**, 469–533 (2017).
8. Argles, T. W., Prince, C. I., Foster, G. L. & Vance, D. New garnets for old? Cautionary tales from young mountain belts. *Earth Planet. Sci. Lett.* **172**, 301–309 (1999).
9. Baxter, E. F. & Scherer, E. E. Garnet Geochronology: timekeeper of tectonometamorphic processes. *Elements* **9**, 433–438 (2013).
10. Caddick, M. J. & Kohn, M. J. Garnet: witness to the evolution of destructive plate boundaries. *Elements* **9**, 427–432 (2013).
11. Maneiro, K. A., Jordan, M. K. & Baxter, E. F. Detrital garnet geochronology. in *Isotopic Constraints on Earth System Processes* 217–236 (American Geophysical Union (AGU), 2022). https://doi.org/10.1002/9781119595007.ch9.
12. Garzanti, E. & Andò, S. Chapter 29 Plate Tectonics and Heavy Mineral Suites of Modern Sands. in *Developments in Sedimentology* (eds. Mange, M. A. & Wright, D. T.) vol. 58, 741–763 (Elsevier, 2007).
13. Garzanti, E. & Andò, S. Heavy minerals for junior woodchucks. *Minerals* **9**, 148 (2019).
14. Smit, M. A., Scherer, E. E. & Mezger, K. Lu–Hf and Sm–Nd garnet geochronology: chronometric closure and implications for dating petrological processes. *Earth Planet. Sci. Lett.* **381**, 222–233 (2013).
15. Smit, M. A. et al. Retentiveness of rare earth elements in garnet with implications for garnet Lu–Hf chronology. *J. Metamorph. Geol.*, 1-25 https://doi.org/10.1111/jmg.12769 (2024).
16. Maneiro, K. A., Baxter, E. F., Samson, S. D., Marschall, H. R. & Hietpas, J. Detrital garnet geochronology: application in tributaries of the French Broad River, Southern Appalachian Mountains, USA. *Geology* **47**, 1189–1192 (2019).
17. Vermeesch, P. How many grains are needed for a provenance study? *Earth Planet. Sci. Lett.* **224**, 441–451 (2004).

18. Millonig, L. J., Albert, R., Gerdes, A., Avigad, D. & Dietsch, C. Exploring laser ablation U–Pb dating of regional metamorphic garnet – The Straits Schist, Connecticut, USA. *Earth Planet. Sci. Lett.* **552**, 116589 (2020).

19. Simpson, A. et al. In-situ Lu-Hf geochronology of garnet, apatite and xenotime by LA ICP MS/MS. *Chem. Geol.* **577**, 120299 (2021).

20. Mark, C. et al. Detrital garnet geochronology by in situ U-Pb and Lu-Hf Analysis: a case study from the European Alps. *J. Geophys. Res.* **128**, e2023JF007244 (2023).

21. Preiss, W. V. Neoproterozoic. in *The Geology of South Australia, Volume 1, The Precambrian* (eds Parker, A. J., Preiss, W. V. & Drexel, J. F.) 171–202 (Geological Survey of South Australia, Adelaide, 1993).

22. Preiss, W. V. Delamerian Orogeny. in *The geology of South Australia, Volume 2, The Phanerozoic* (eds Parker, A. J., Preiss, W. V. & Drexel, J. F.) 45–59 (Geological Survey of South Australia, Adelaide, 1995).

23. Preiss, W. V. The adelaide geosyncline of South Australia and its significance in neoproterozoic continental reconstruction. *Precambrian Res.* **100**, 21–63 (2000).

24. Foden, J., Elburg, M. A., Dougherty-Page, J. & Burtt, A. The timing and duration of the delamerian orogeny: correlation with the Ross Orogen and Implications for Gondwana assembly. *J. Geol.* **114**, 189–210 (2006).

25. Szpunar, M. et al. Timing of Proterozoic high-grade metamorphism in the Barossa Complex, southern South Australia: exploring the extent of the 1590 Ma event Barossa Complex, 1590 Ma metamorphic event. *MESA J.* **47**, 21–27 (2007).

26. Meaney, K. J. Proterozoic crustal growth in the southeastern Gawler Craton: the development of the Barossa Complex, and an assessment of the detrital zircon method. (University of Adelaide, School of Physical Sciences, 2018).

27. Foden, J. et al. Cambro-Ordovician magmatism in the Delamerian orogeny: Implications for tectonic development of the southern Gondwanan margin. *Gondwana Res.* **81**, 490–521 (2020).

28. Reid, A. et al. Complex 40Ar/39Ar age spectra from low-grade metamorphic rocks: resolving the input of detrital and metamorphic components in a case study from the Delamerian Orogen. *Geochronology* **4**, 471–500 (2022).

29. Alley, N. F. & Bourman, R. P. Troubridge Basin. in *The Geology of South Australia, Volume 2, the Phanerozoic* (eds. Parker, A. J., Preiss, W. V. & Drexel, J. F.) 65–70 (The Geological Survey of South Australia, Adelaide, 1995).

30. Alley, N. F., Bourman, R. P. & Milnes, A. R. Late Paleozoic Troubridge Basin sediments on Kangaroo Island, South Australia. *MESA J.* **70**, 24–43 (2013).

31. Simpson, A., Glorie, S., Hand, M., Spandler, C. & Gilbert, S. Garnet Lu-Hf speed dating: a novel method to rapidly resolve polymetamorphic histories. *Gondwana Res.* **121**, 215–234 (2023).

32. Glorie, S., Simpson, A., Gilbert, S. E., Hand, M. & Müller, A. B. Testing the reproducibility of in situ LuHf dating using Lu-rich garnet from the Tørdal pegmatites, southern Norway. *Chem. Geol.* **653**, 122038 (2024).

33. Lane, K. Metamorphic and geochronological constraints on the evolution of the Kalinjala Shear Zone, Eyre Peninsula. (2011).

34. Jagodzinski, E., Szpunar, M., Meaney, K. & Fraser, G. *SHRIMP U-Pb Dating of the Barossa Complex, South Australia: Exploring Tectonic Links between the Gawler Craton and Curnamona Province* (2020).

35. Morrissey, L. J., Hand, M., Wade, B. P. & Szpunar, M. Early Mesoproterozoic metamorphism in the Barossa Complex, South Australia: links with the eastern margin of Proterozoic Australia. *Aust. J. Earth Sci.* **60**, 769–795 (2013).

36. Schönig, J., von Eynatten, H., Tolosana-Delgado, R. & Meinhold, G. Garnet major-element composition as an indicator of host-rock type: a machine learning approach using the random forest classifier. *Contrib. Miner. Pet.* **176**, 98 (2021).

37. Krippner, A., Meinhold, G., Morton, A. C. & von Eynatten, H. Evaluation of garnet discrimination diagrams using geochemical data of garnets derived from various host rocks. *Sediment. Geol.* **306**, 36–52 (2014).

38. Alley, N. F. et al. Late Palaeozoic. in *The geology of South Australia, Volume 2, The Phanerozoic* (eds Drexel, J. F. & Preiss, W. V.) 63–91 (South Australia, Adelaide, 1995).

39. Isbell, J. L. et al. Glacial paradoxes during the late Paleozoic ice age: evaluating the equilibrium line altitude as a control on glaciation. *Gondwana Res.* **22**, 1–19 (2012).

40. Isbell, J. L. et al. Evaluation of physical and chemical proxies used to interpret past glaciations with a focus on the late Paleozoic Ice Age. *Earth Sci. Rev.* **221**, 103756 (2021).

41. Granmayeh, A. *Petrology and Provenance of Permian Glaciogenic Sediments of Southern Australia*. (University of Adelaide, Adelaide, 1994).

42. Normington, V., Hill, S., Tiddy, C. & Giles, D. *Sedimentology of the Late Palaeozoic Cape Jervis Formation, Troubridge Basin, South Australia. Geological Survey of South Australia* (2018).

43. Goodge, J. W. Geological and tectonic evolution of the Transantarctic Mountains, from ancient craton to recent enigma. *Gondwana Res.* **80**, 50–122 (2020).

44. Goodge, J. W., Fanning, C. M., Norman, M. D. & Bennett, V. C. Temporal, isotopic and spatial relations of early paleozoic Gondwana-Margin Arc Magmatism, Central Transantarctic Mountains, Antarctica. *J. Petrol.* **53**, 2027–2065 (2012).

45. Hagen-Peter, G., Cottle, J. M., Tulloch, A. J. & Cox, S. C. Mixing between enriched lithospheric mantle and crustal components in a short-lived subduction-related magma system, Dry Valleys area, Antarctica: Insights from U-Pb geochronology, Hf isotopes, and whole-rock geochemistry. *Lithosphere* **7**, 174–188 (2015).

46. Goodge, J. W., Williams, I. S. & Myrow, P. Provenance of Neoproterozoic and lower Paleozoic siliciclastic rocks of the central Ross orogen, Antarctica: detrital record of rift-, passive-, and active-margin sedimentation. *GSA Bull.* **116**, 1253–1279 (2004).

47. Cooper, A. F., Maas, R., Scott, J. M. & Barber, A. J. W. Dating of volcanism and sedimentation in the Skelton Group, Transantarctic Mountains: implications for the Rodinia-Gondwana transition in southern Victoria Land, Antarctica. *GSA Bull.* **123**, 681–702 (2011).

48. Goodge, J. W., Myrow, P., Williams, I. S. & Bowring, S. A. Age and Provenance of the Beardmore Group, Antarctica: Constraints on Rodinia Supercontinent Breakup. *J. Geol.* **110**, 393–406 (2002).

49. Goodge, J. W., Walker, N. W. & Hansen, V. L. Neoproterozoic-Cambrian basement-involved orogenesis within the Antarctic margin of Gondwana. *Geology* **21**, 37–40 (1993).

50. Goodge, J. W. & Fanning, C. M. Composition and age of the East Antarctic Shield in eastern Wilkes Land determined by proxy from Oligocene-Pleistocene glaciomarine sediment and Beacon Supergroup sandstones, Antarctica. *GSA Bull.* **122**, 1135–1159 (2010).

51. Paulsen, T. S., Deering, C., Sliwinski, J., Bachmann, O. & Guillong, M. Detrital zircon ages from the Ross Supergroup, north Victoria Land, Antarctica: implications for the tectonostratigraphic evolution of the Pacific-Gondwana margin. *Gondwana Res.* **35**, 79–96 (2016).

52. Lamarque, G. et al. Ediacaran to lower Cambrian basement in eastern George V Land (Antarctica): evidence from UPb dating of gneiss xenoliths and implications for the South Australia-East Antarctica connection. *Lithos* **318–319**, 219–229 (2018).

53. Grindley, G. W. & McDougall, I. Age and correlation of the Nimrod Group and other precambrian rock units in the central Transantarctic Mountains, Antarctica. *N.Z. J. Geol. Geophys.* **12**, 391–411 (1969).

54. Goodge, J. W. Latest Neoproterozoic basin inversion of the Beardmore Group, central Transantarctic Mountains, Antarctica. *Tectonics* **16**, 682–701 (1997).

55. Myrow, P. M., Pope, M. C., Goodge, J. W., Fischer, W. & Palmer, A. R. Depositional history of pre-Devonian strata and timing of Ross orogenic tectonism in the central Transantarctic Mountains, Antarctica. *GSA Bull.* **114**, 1070–1088 (2002).

56. Hagen-Peter, G., Cottle, J. M., Smit, M. & Cooper, A. F. Coupled garnet Lu–Hf and monazite U–Pb geochronology constrain early

convergent margin dynamics in the Ross orogen, Antarctica. *J. Metamorph. Geol.* **34**, 293–319 (2016).

57. Rocchi, S., Bracciali, L., Di Vincenzo, G., Gemelli, M. & Ghezzo, C. Arc accretion to the early Paleozoic Antarctic margin of Gondwana in Victoria Land. *Gondwana Res.* **19**, 594–607 (2011).

58. Hagen-Peter, G. & Cottle, J. M. Synchronous alkaline and subalkaline magmatism during the late Neoproterozoic–early Paleozoic Ross orogeny, Antarctica: insights into magmatic sources and processes within a continental arc. *Lithos* **262**, 677–698 (2016).

59. Cottle, J. M. & Cooper, A. F. Geology, geochemistry, and geochronology of an A-type granite in the Mulock Glacier area, southern Victoria Land, Antarctica. *N.Z. J. Geol. Geophys.* **49**, 191–202 (2006).

60. Cawood, P. A. Terra Australis Orogen: Rodinia breakup and development of the Pacific and Iapetus margins of Gondwana during the Neoproterozoic and Paleozoic. *Earth Sci. Rev.* **69**, 249–279 (2005).

61. Glen, R. A. & Cooper, R. A. Evolution of the East Gondwana convergent margin in Antarctica, southern Australia and New Zealand from the Neoproterozoic to latest Devonian. *Earth Sci. Rev.* **220**, 103687 (2021).

62. Mulder, J. A. et al. Neoproterozoic opening of the Pacific Ocean recorded by multi-stage rifting in Tasmania, Australia. *Earth Sci. Rev.* **201**, 103041 (2020).

63. Mason, D. R. *Mineralogy of Heavy Mineral Separates from Sediments of Kangaroo Island, South Australia, Open File Envelope 12420, Mason Geoscience Pty Ltd. Department for Manufacturing, Innovation, Trade, Resources and Energy, South Australia, Adelaide* (2002).

64. Tamblyn, R. et al. In situ laser ablation Lu–Hf geochronology of garnet across the Western Gneiss Region: campaign-style dating of metamorphism. *J. Geol. Soc.* https://doi.org/10.1144/JGS2021-094 (2021).

65. Brown, D. A. et al. Laser-ablation Lu-Hf dating reveals Laurentian garnet in subducted rocks from southern Australia. *Geology* **50**, 837–842 (2022).

66. Nebel, O., Morel, M. L. A. & Vroon, P. Z. Isotope dilution determinations of Lu, Hf, Zr, Ta and W, and Hf isotope compositions of NIST SRM 610 and 612 glass wafers. *Geostand. Geoanal. Res.* **33**, 487–499 (2009).

67. Jochum, K. P. et al. Determination of reference values for NIST SRM 610–617 glasses following ISO guidelines. *Geostand. Geoanal. Res.* **35**, 397–429 (2011).

68. Norris, A. & Danyushevsky, L. Towards estimating the complete uncertainty budget of quantified results measured by LA-ICP-MS. in *Goldschmidt* (Boston, 2018).

69. Larson, K. P. et al. Investigating low dispersion isotope dissolution Lu-Hf garnet dates via in situ Lu-Hf geochronology, Kanchenjunga Himal. *Geosci. Front.* **15**, 101781 (2024).

70. Romer, R. L. & Smeds, S.-A. U-Pb columbite ages of pegmatites from Sveconorwegian terranes in southwestern Sweden. *Precambrian Res.* **76**, 15–30 (1996).

71. Li, Y. & Vermeesch, P. Short communication: Inverse isochron regression for Re–Os, K–Ca and other chronometers. *Geochronology* **3**, 415–420 (2021).

72. Glorie, S. et al. Detrital apatite Lu–Hf and U–Pb geochronology applied to the southwestern Siberian margin. *Terra Nova*. https://doi.org/10.1111/TER.12580 (2022).

73. Fisher, C. M. & Vervoort, J. D. Using the magmatic record to constrain the growth of continental crust—the Eoarchean zircon Hf record of Greenland. *Earth Planet. Sci. Lett.* **488**, 79–91 (2018).

74. Spencer, C. J., Kirkland, C. L., Roberts, N. M. W., Evans, N. J. & Liebmann, J. Strategies towards robust interpretations of in situ zircon Lu–Hf isotope analyses. *Geosci. Front.* **11**, 843–853 (2020).

75. Vermeesch, P. IsoplotR: a free and open toolbox for geochronology. *Geosci. Front.* **9**, 1479–1493 (2018).

76. Spencer, C. J., Kirkland, C. L. & Taylor, R. J. M. Strategies towards statistically robust interpretations of in situ U–Pb zircon geochronology. *Geosci. Front.* **7**, 581–589 (2016).

77. Horstwood, M. S. A. et al. Community-derived standards for LA-ICP-MS U-(Th-)Pb geochronology—uncertainty propagation, age interpretation and data reporting. *Geostand. Geoanal. Res.* **40**, 311–332 (2016).

78. Sláma, J. et al. Plešovice zircon—a new natural reference material for U–Pb and Hf isotopic microanalysis. *Chem. Geol.* **249**, 1–35 (2008).

79. Preiss, W. V., Fanning, C., Szpunar, M. A. & Burtt, A. C. Age and tectonic significance of the Mount Crawford Granite Gneiss and a related intrusive in the Oakbank Inlier, Mount Lofty Ranges, South Australia. *MESA J.* **49**, 38–49 (2008).

80. Cowley, W. M., compiler. Geological Map South Australia: Department for Energy and Mining, scale 1:2,000,000. (2020).

81. Lawver, L. A., Dalziel, I. W. D., Norton, I. O., Gahagan, L. M. & Davis, J. The PLATES 2014 Atlas of Plate Reconstructions (550 Ma to Present Day), PLATES Progress Report No. 374-0215. *University of Texas Institute for Geophysics Technical Report No. 202* 220. https://doi.org/10.15781/T20V8B147 (2015).

82. Stutenbecker, L., Berger, A. & Schlunegger, F. The potential of detrital garnet as a provenance proxy in the Central Swiss Alps. *Sediment. Geol.* **351**, 11–20 (2017).

83. Goodge, J. W. & Finn, C. A. Glimpses of East Antarctica: aeromagnetic and satellite magnetic view from the central Transantarctic Mountains of East Antarctica. *J. Geophys. Res.* **115**, B09103 (2010).

84. Reid, A. J. & Hand, M. Mesoarchean to Mesoproterozoic evolution of the southern Gawler Craton, South Australia. *Epis. J. Int. Geosci.* **35**, 216–225 (2012).

85. Gibson, G. M. et al. Pre-existing basement structure and its influence on continental rifting and fracture zone development along Australia's southern rifted margin. *J. Geol. Soc.* **170**, 365–377 (2013).

86. Glen, R. A. et al. Geodynamic significance of the boundary between the Thomson Orogen and the Lachlan Orogen, northwestern New South Wales and implications for Tasmanide tectonics. *Aust. J. Earth Sci.* **60**, 371–412 (2013).

87. Brown, D. A., Hand, M., Morrissey, L. J. & Goodge, J. W. Cambrian eclogite-facies metamorphism in the central Transantarctic Mountains, East Antarctica: extending the record of early Palaeozoic high-pressure metamorphism along the eastern Gondwanan margin. *Lithos* **366–367**, 105571 (2020).

Author contributions

S.V.: conceptualisation, formal analysis, data processing, data interpretation, visualisation, writing—paper drafting; S.G.: funding acquisition, conceptualisation, data interpretation, writing—paper editing, primary supervision; M.H.: funding acquisition, conceptualisation, providing samples, data interpretation, writing—paper editing, supervision; J.M.: data interpretation, writing—paper editing; A.M.: providing samples, writing—paper editing; J.H.: data interpretation, writing—paper editing, supervision.

Competing interests

The authors declare no competing interests.

Additional information